Condensed-Phase Effects on the Structural Properties of $C_6H_5CN-BF_3$ and $(CH_3)_3CCN-BF_3$: IR Spectra, Crystallography, and Computations

J. A. Phillips,*,† D. J. Giesen,‡ N. P. Wells,† J. A. Halfen,† C. C. Knutson,† and J. P. Wrass†

Department of Chemistry, University of Wisconsin—Eau Claire, 105 Garfield Ave., Eau Claire, Wisconsin 54701 and Research Laboratories, Eastman Kodak Company, Rochester, New York 14650-2109

Received: May 12, 2005; In Final Form: June 16, 2005

Condensed-phase effects on the structure and bonding of $C_6H_5CN-BF_3$ and $(CH_3)_3CCN-BF_3$ are illustrated by a variety of results, and these are compared to analogous data for the closely related complex CH_3CN-BF_3. For the most part, the structural properties of $C_6H_5CN-BF_3$ and $(CH_3)_3CCN-BF_3$ are quite similar, not only in the gas phase but also in the solid state and in argon matrices. However, the structures do change significantly from medium to medium, and these changes are reflected in the data presented below. Specifically, the measured crystallographic structure of $C_6H_5CN-BF_3$ (s) has a B−N distance that is 0.17 Å shorter than that in the equilibrium gas-phase structure obtained via B3LYP calculations. Notable differences between calculated gas-phase frequencies and measured solid-state frequencies for both $C_6H_5CN-BF_3$ and $(CH_3)_3CCN-BF_3$ were also observed, and in the case of $(CH_3)_3CCN-BF_3$, these data implicate a comparable difference between solid-state and gas-phase structure, even in the absence of crystallographic results. Frequencies measured in argon matrices were found to be quite similar for both complexes and also very near those measured previously for CH_3CN-BF_3, suggesting that all three complexes adopt similar structures in solid argon. For $C_6H_5CN-BF_3$ and $(CH_3)_3CCN-BF_3$, matrix IR frequencies differ only slightly from the computed gas-phase values, but do suggest a slight compression of the B−N bond. Ultimately, it appears that the varying degree to which these systems respond to condensed phases stems from subtle differences in the gas-phase species, which are highlighted through an examination of B−N distance potentials from B3LYP calculations. The larger organic substituents appear to stabilize the potential near 1.8 Å, so that the structures are more localized in that region prior to any condensed-phase interactions. As a result, the condensed-phase effects on the structural properties of $C_6H_5CN-BF_3$ and $(CH_3)_3CCN-BF_3$ are much less pronounced than those for CH_3CN-BF_3.

I. Introduction

The structural chemistry of nitrile−boron trifluoride complexes has been the subject of numerous studies over the past few decades.[1−17] Recent interest has stemmed in part from the observation that gas-phase structures of these systems depict interactions that defy classification as purely bonding or nonbonding interactions.[1] Furthermore, these structures change dramatically upon crystallization; the B−N dative bond shortens, and accordingly, the N−B−F angle increases as well.[1,2] For example, the experimental gas-phase structure of CH_3CN-BF_3 has a B−N distance of 2.01 Å and an N−B−F angle of 95.6°.[3] Clearly, these structural parameters are very much intermediate between those observed for strong complexes such as H_3N-BF_3[4] and "van der Waals complexes" like N_2-BF_3[5] or $NCCN-BF_3$,[6] for which gas-phase B−N distances are listed in Table 1 below (together with proton affinity values for the nitrogen donors). In the solid state, however, the B−N distance of CH_3CN-BF_3 is 1.65 Å and the N−B−F angle is 105.6°,[7] much like H_3N-BF_3. Thus, crystallization causes the B−N distance to contract by about 0.4 Å, and the N−B−F angle to open by 10°. For $HCN-BF_3$, the gas-phase B−N distance is 2.47 Å,[8] but contracts nearly 0.8 Å upon crystallization to 1.64 Å.[9]

TABLE 1: Proton Affinities of Various Nitrogen Donors, and B−N Distances in Their Respective BF_3 Complexes

molecule	proton affinity[a]	R(B−N)[b]
NH_3	853.6	1.673(10)[c]
C_6H_5CN	811.5	1.798[d]
$(CH_3)_3CCN$	810.9	1.778[d]
CH_3CN	779.2	2.011(7)[e]
$ClCH_2CN$	745.7	
HCN	712.9	2.473(29)[f]
NCCN	674.7	2.647(3)[g]
N_2	493.8	2.875(2)[h]

[a] $-\Delta H$ values (in kJ/mol) for the reaction B (g) + H^+ (g) → HB^+ (g). From ref 18. [b] In units of Å and from experimental data, except for those obtained in this work. [c] Ref 4. [d] This work. [e] Experimental, vibrationally-averaged value from ref 3. The calculated equilibrium distance is 1.868 Å at the B3LYP/aug-cc-pVTZ level, and 2.315 Å at the B3LYP/aug-cc-pVQZ level. [f] Ref 8. [g] Ref 6. [h] Ref 5.

Such large differences between gas and solid-state structures raise the question as to how a solvent or other bulk, condensed-phase medium may affect these systems. While there is no direct method by which precise structural properties can be measured in solution, IR frequency shifts have offered some semiquantitative insight. A few early studies focused on shifts of the CN stretching band of CH_3CN-BF_3 in various solvents,[10] but

* Corresponding author. E-mail: phillija@uwec.edu. Telephone: 715-836-5399. Fax: 715-836-4979.
† University of Wisconsin—Eau Claire.
‡ Eastman Kodak Company.

10.1021/jp052495q CCC: $30.25 © 2005 American Chemical Society
Published on Web 08/19/2005

surprisingly, the observed frequencies (~2355 cm^{-1}) are largely solvent independent. Our work has been concerned with the effects of inert, cryogenic matrices, and we have focused on vibrational modes involving motions in the BF_3 moiety, which are quite sensitive to structural changes. Frequencies of CH_3CN-BF_3 measured in solid argon[11] are significantly different from those measured for pure solid CH_3CN-BF_3,[12] and the shifts are consistent with the notion that the matrix-isolated complex is more weakly bonded and has a longer B−N distance than its crystalline counterpart. Experimental gas-phase frequencies have yet to be measured, but frequencies were calculated for two minimum-energy structures with B−N distances of 1.92 and 2.32 Å (see below).[13] Ultimately, all matrix frequencies were found to be bracketed by the solid-state data and those calculated for the 1.92 Å structure, indicating that the matrix environment does induce substantial structural changes in CH_3CN-BF_3, though not the extent that occurs in the crystal.

Prior to our matrix work, several computational studies of CH_3CN-BF_3 had been conducted, and surprisingly, two distinctly different types of structures had been obtained, one with a B−N distance of about 1.8 Å[14] and three others with B−N distances between 2.2 and 2.3 Å.[15−17] Moreover, all compared quite poorly to the experimental structure, although they were conducted at the MP2 level of theory with reasonably large basis sets. Regardless, the lack of agreement precluded any valid comparison between our measured, argon-matrix frequencies and those calculated for the 1.8 Å structure.[14] In turn, we reexamined CH_3CN-BF_3 using both MP2 and B3LYP calculations and larger basis sets, in hopes of resolving the experiment-theory structure discrepancy and obtaining reliable gas-phase frequencies.[13] Surprisingly, we were also unable to reproduce the experimental structure, but did obtain structures very much like *both* of those reported in the previous computational studies. The key was the inclusion of diffuse functions in the basis set (signified by "aug" or "+"). With them, shorter B−N distances near 1.8 Å were obtained; without them, longer B−N distances near 2.3 Å were obtained. The exception was the structure obtained with the largest basis set (B3LYP/aug-cc-pVQZ), which had an equilibrium distance of 2.315 Å, despite the diffuse functions. The underlying peculiarity was a very flat B−N distance potential, and in several cases, including B3LYP/aug-cc-pVQZ, it exhibited two distinct minima roughly corresponding to each type of structure obtained previously. Ultimately, it was inferred that the experiment-theory structure discrepancy was most likely genuine, and stemmed from a large amplitude zero-point motion in the B−N stretching mode that resulted in a bona fide difference between the experimental (vibrationally averaged) and theoretical (equilibrium) structures.[13]

This work represents our first step toward identifying other systems with remarkable structural features akin to those of CH_3CN-BF_3. At this point, we turn to the BF_3 complexes of nitrile donors with larger organic substituents, specifically trimethyl acetonitrile ($(CH_3)_3CCN$) and benzonitrile (C_6H_5CN). Table 1 shows gas-phase proton affinity values[18] for these compounds and a handful of other nitriles, together with ammonia and N_2 as reference points for fairly strong and very weak Lewis bases, respectively. These data illustrate that the species with larger organic substituents are indeed stronger bases than CH_3CN, but they are still weaker than NH_3. Below, we present a myriad of structural data for these complexes, including gas-phase structures, frequencies, and B−N distance potentials from B3LYP computations, IR spectra from argon matrices and thin films of the bulk solids, and an X-ray structure for $C_6H_5CN-BF_3$. Together, these results show that $(CH_3)_3CCN-BF_3$ and $C_6H_5CN-BF_3$ are rather sensitive to condensed-phase media, but the effects are somewhat muted relative to CH_3CN-BF_3.

TABLE 2: X-ray Crystallographic Data for $C_6H_5CN-BF_3$[a]

empirical formula	$C_7H_5BF_3N$
formula weight	170.93
crystal system	orthorhombic
space group	*Pnma*
A (Å)	17.404(2)
B (Å)	8.678(2)
c (Å)	4.856(1)
V (Å^3)	733.4(2)
Z	4
temperature (K)	100
calculated density (g cm^{-3})	1.548
crystal size (mm)	0.45 × 0.40 × 0.35
absorption coefficient (mm^{-1})	0.144
2θ max (deg)	52.10
no. of reflections collected	764
no. of independent reflections	763
no. of reflections with $I > 2\sigma(I)$	668
no. of variables	75
R1 (wR2) [$I > 2\sigma(I)$] [b]	0.0378 (0.1036)
R1 (wR2) [all data]	0.0432 (0.1079)
GOF	1.118
difference peaks (e^- Å^{-3})	0.234, −0.263

[a] See Experimental Section for additional data collection, reduction, structure solution, and refinement details. [b] $R1 = \Sigma\,||F_o| - |F_c||/\Sigma\,|F_o|$; $wR2 = [\Sigma[w(F_o^2 - F_c^2)^2]]^{1/2}$, where $w = 1/\sigma^2(F_o^2) + (aP)^2 + bP$.

II. Experimental Section

Materials. $(CH_3)_3CCN$ (98%) and C_6H_5CCN (99+%) were obtained from Aldrich and were subjected to a few freeze−pump−thaw cycles prior to use. BF_3 (99.5+%) was also obtained from Aldrich, and other gases, including argon (99.9995%) and N_2 (standard purity), were obtained from Praxair. All gases were used without further purification

Preparation of Crystalline Samples. Solid samples of $C_6H_5CN-BF_3$ and $(CH_3)_3CN-BF_3$ were prepared by first adding about 5 mL of liquid nitrile to a 50- or 100-mL Schlenk tube. The top of the tube was fitted with a rubber septum. Gases were introduced through the septum via a small hypodermic needle and were allowed to vent through a sidearm (and into a fume hood) by slightly opening a Teflon stopcock. Initially, the tube was purged with a steady flow of N_2 for several minutes to displace residual air. Then, BF_3 was slowly introduced to the tube in a similar manner. Immediately, a white solid formed, and the tube became somewhat warm. The BF_3 flow was continued for a few additional minutes to ensure that nearly all the nitrile had reacted, and it was clear (via white fumes from the sidearm) that the BF_3 had displaced most of the nitrogen. The excess BF_3 was allowed to remain in the tube, and the sample was sealed and placed in a desiccator for several days to allow crystal growth. The compounds were apt to decompose rapidly in air, presumably because of the reaction with ambient water vapor. Because of this, samples were cooled to 0 °C and immersed in oil prior to mounting on the diffractometer needle.

Crystallography. A colorless block crystal of $C_6H_5CN-BF_3$ with dimensions of 0.45 mm × 0.40 mm × 0.35 mm was cleaved from a larger sample and transferred to a Bruker/Nonius MACH3S diffractometer equipped with graphite-monochromated Mo Kα radiation ($\alpha = 0.71073$ Å) for a data collection at 100 K. Relevant crystallographic information is given in Table 2. Unit cell constants were determined from a least-squares refinement of the setting angles of 25 machine-centered reflec-

tions in the range $9.98° < \theta < 25.71°$. Intensity data were collected using the $\omega/2\theta$ scan technique to a maximum 2θ value of 52.10°. The intensity data were corrected for Lorentz and polarization effects and converted to structure factors using the program XCAD4.[19]

The space group *Pnma* was determined on the basis of systematic absences and intensity statistics. A successful direct-methods solution was calculated that provided the positions of most of the non-hydrogen atoms directly from the E-map. The remaining non-hydrogen atoms were located after several cycles of structure expansion and full-matrix least-squares refinement. Hydrogen atoms were added geometrically. All non-hydrogen atoms were refined with anisotropic displacement parameters. Hydrogen atoms were refined as riding atoms with group isotropic displacement parameters fixed at $1.2 \times U(\text{eq})$ of the host carbon atom. The final difference map was featureless, with the largest residual peak ($0.23\ e^-\ Å^{-3}$) located 0.64 Å from C2. Structure solution and refinement calculations were performed using the SHELXTL suite of programs.[20] Complete crystallographic information in CIF format is provided as Supporting Information (Table S1).

Several crystalline samples of $(CH_3)_3CCN-BF_3$, similar in size to those of $C_6H_5CN-BF_3$ were also obtained; however, these either decomposed or underwent a phase transition en route to lower temperatures. As such, an insufficient number of reflections were obtained for $(CH_3)_3CCN-BF_3$, and a structure determination was not possible.

Infrared Spectra. All infrared spectra were collected using a Cryomech ST15 optical cryostat fitted with KBr windows (both internal and external). Temperature was measured and controlled using a Scientific Instruments 9600-1 temperature controller and a single Si diode located at the end of the second refrigeration stage. As such, the actual sample temperature is probably a few degrees warmer than that indicated by the controller. Spectra were recorded using a Nicolet Avatar 360 FTIR at 1.0 cm^{-1} resolution, and typically, 100 scans were averaged for both sample and background data. The observed peak maxima were reproducible to ± 1 cm^{-1} for matrix experiments, and about ± 5 cm^{-1} for bulk solid measurements. The cryostat apparatus is assembled on a movable cart, which is wheeled into the spectrometer sample compartment for each spectrum. As such, interference from residual water and CO_2 in the unpurged beam path can be problematic on occasion. Separate gas mixtures containing either the nitrile species or BF_3 were flowed into the cryostat vacuum chamber utilizing a concentric, dual-deposition flange described previously.[11] This design enables controlled mixing of reactive gas mixtures immediately prior to the point that they enter the cryostat vacuum chamber.

Matrix IR spectra of $(CH_3)_3CCN-BF_3$ were obtained by codepositing separate mixtures of BF_3 in argon and $(CH_3)_3CCN$ in argon, for which guest-to-host ratios ranged from $^1/_8$ to 1%. Because C_6H_5CN has a vapor pressure below 1 Torr, it was difficult to make gas mixtures rich enough in C_6H_5CN at a total pressure above 1 atm. As such, most of these experiments were conducted with a sample tube containing the pure liquid attached directly to the deposition line, while a BF_3/argon mixture was deposited via the other line. Peaks due to the 1:1 complex were much clearer in these spectra, but the concentration of C_6H_5CN in the matrix was somewhat uncertain, though it could be controlled via fine adjustment of a needle valve. Matrices were deposited at temperatures between 9 and 14 K, with deposition rates ranging from 3 to 10 mmol/h. Typically, 2−4 successive depositions were performed over several hours, and spectra were recorded after each one. Optimal signals were obtained with a deposition rate of about 5 mmol/h and host concentrations in the individual gas mixtures of about 0.25%. When two mixtures were deposited at roughly equal rates, the final composition of the matrix sample was about 1:1:800 (BF_3/nitrile/argon). Most samples were subsequently annealed to approximately 25−30 K for 30−60 min to facilitate complex formation and aid in the identification of peaks. A few samples were annealed to higher temperatures for the purpose of identifying peaks due to larger aggregates. IR spectra of the bulk, solid complexes were obtained by codepositing the gas mixtures in a manner similar to the matrix experiments, except that the cold window was held at a much warmer temperature, typically 100 K, such that the host gas did not condense. These spectra closely resemble low-temperature, solid-state IR spectra of CH_3CN-BF_3,[12] indicating that majority of the sample consists of nitrile−BF_3 complexes, though excess, unreacted BF_3 was also observed in some experiments.

III. Computational Methods

All calculations were performed using either *Gaussian 98*[21] or *Gaussian 03*.[22] To determine the effect of basis set size, a variety of basis sets were explored including 3-21G,[23] MIDI!,[24] 6-31G*,[25] 6-31+G*,[25] 6-311G*,[26,27] 6-311+G*,[26,27] cc-pVDZ,[28] aug-cc-pVDZ,[28] cc-pVTZ,[28] aug-cc-pVTZ,[28] and aug-cc-pVQZ.[28] For aug-cc-pVTZ and aug-cc-pVQZ, a mixed basis set was used as follows: the large basis set was used on five atoms, the BF_3 group plus the nitrile C and N, and aug-cc-pVDZ was used on all other atoms. These two mixed basis sets will be referred to as aug-cc-pV(T|D)Z and aug-cc-pV(Q|D)Z. When appropriate, symmetry was used, C_{3v} for $(CH_3)_3CCN-BF_3$ and C_s for $C_6H_5CN-BF_3$. B−N distance potentials were computed by constraining the B−N distance to a specific value and optimizing all other degrees of freedom. Such points were calculated every 0.1 Å between 1.6 and 2.5 Å, inclusive. Because of the shallow B−N potential energy surfaces for these molecules, minimum-energy conformations were computed by optimizing all degrees of freedom using the OPT = TIGHT option, which tightens the optimization criteria by a factor of 30, and frequencies were calculated to ensure a minimum had been found. In the case of $(CH_3)_3CCN-BF_3$, the structure with the *tert*-butyl carbons eclipsing the fluorine atoms showed a very small negative (i.e., imaginary) frequency of -3 cm^{-1}, while the structure with the C and F atoms staggered showed a very small positive frequency of $+3$ cm^{-1}. Attempts were made to find a nonsymmetric minimum for $C_6H_5CN-BF_3$ such as that seen in the crystal structure, but the tilted geometry optimized to a structure with a C−N−B angle greater than 179.9° under normal convergence criteria. Attempts to refine this structure with OPT = TIGHT to determine whether the structure was truly linear about the C−N−B angle were unsuccessful at achieving convergence at the specified criteria, but the geometry remained very close to 180°. Isotope effects on the frequencies were computed by comparing the frequencies calculated with the default ^{11}B isotope to those calculated using ^{10}B. The other isotopes used in the frequency calculations were ^1H, ^{12}C, ^{14}N, and ^{19}F.

IV. Results & Discussion

Structure. Equilibrium gas-phase structures for $C_6H_5CN-BF_3$ and $(CH_3)_3CCN-BF_3$ obtained from B3LYP/aug-cc-pV(T|D)Z calculations are displayed in Figure 1. As a whole, these structures are quite similar, with the $(CH_3)_3CCN$ complex having a slightly shorter B−N distance. In turn, the $(CH_3)_3CCN-$

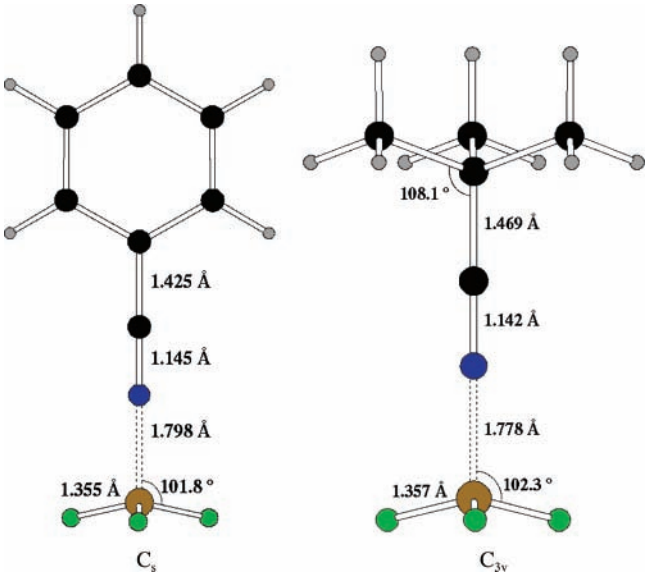

Figure 1. B3LYP/aug-cc-pV(T|D)Z[a] Structures of $C_6H_5CN-BF_3$ and $(CH_3)_3CCN-BF_3$.

BF_3 structure has a somewhat larger N−B−F angle, and the B−F bonds are slightly longer as well. It is worth noting that these differences, though very minor, are opposite of what would be expected on the basis of the (perhaps negligible) difference in proton affinity values,[18] but are consistent with the intuitive notion that the *tert*-butyl substituent is slightly more electron-releasing than a phenyl group. Regardless, both structures do resemble those obtained for CH_3CN-BF_3 when diffuse functions were included in the basis set (except in the case of the largest basis set: aug-cc-pVQZ).[13] It is worth noting again, however, that the experimental, vibrationally averaged structure of CH_3CN-BF_3 has a B−N distance of 2.01 Å,[3] and the equilibrium structure at the B3LYP/aug-cc-pVQZ level has a B−N distance of 2.315 Å.[13] The most reasonable structure for comparison is the B3LYP/aug-cc-pVTZ result for CH_3CN-BF_3,[13] which has a B−N distance of 1.868 Å, an N−B−F angle of 95.9°, and B−F distances of 1.328 Å. Thus, the appropriate CH_3CN-BF_3 data suggest a complex that is just slightly less strongly bonded than $C_6H_5CN-BF_3$ and $(CH_3)_3CCN-BF_3$, which is consistent with both intuition and proton affinity data.[19]

The solid-state structure of $C_6H_5CN-BF_3$ is shown in Figure 2, and despite the differences in proton affinity values among HCN, CH_3CN, and C_6H_5CN, it very much resembles the crystal structures of $HCN-BF_3$[9] and CH_3CN-BF_3.[7] Clearly, however, it does differ markedly from the calculated gas-phase structure, as the B−N distance is 0.17 Å shorter, and the N−B−F angle is about 3° larger. While these differences are less extreme than those observed previously for $HCN-BF_3$ (ΔR(B−N) = 0.8 Å)[9] and CH_3CN-BF_3 (ΔR(B−N) = 0.4 Å),[3] they are still considerably larger than those observed in most instances (typically 0.01 Å).[2] One other somewhat peculiar aspect of the structure is that it is bent slightly about the C−N−B linkage. No evidence of a bent minimum-energy structure was found in the computations, which seems to rule out any intramolecular effect, although it is worth pointing out that the π_{CN}-type orbitals are not degenerate in benzonitrile (C_s), as they are in the case of the higher-symmetry (C_{3v}) donors such as acetonitrile. Thus, in principle, a slight bend could enhance overlap with the higher-energy π_{CN} orbital in some cases.

On the other hand, it is probable that the slight bend of the C−N−B unit is due to an intermolecular B−F···H interaction. Each of the three BF_3 fluorine atoms participates as an acceptor in a B−F···H "hydrogen bond", ranging in length from 2.41 to 2.44 Å. The latter of these two interactions, between F(1) and a *para*-hydrogen atom of a neighboring $C_6H_5CN-BF_3$ unit, is the likely origin of the bend in the C−N−B unit (Figure 3), as establishment of this nearly linear B−F···H interaction would displace the boron atom from the N(1)≡C(1)−C(2) vector. A search of the Cambridge Structural Database reveals 39 previous instances of B−F···H interactions in which a benzonitrile hydrogen atom serves as the "hydrogen bond" donor, ranging in length from 2.36 to 2.59 Å.[29] Weak B−F···H interactions in which BF_3 serves as the "hydrogen bond" acceptor are less

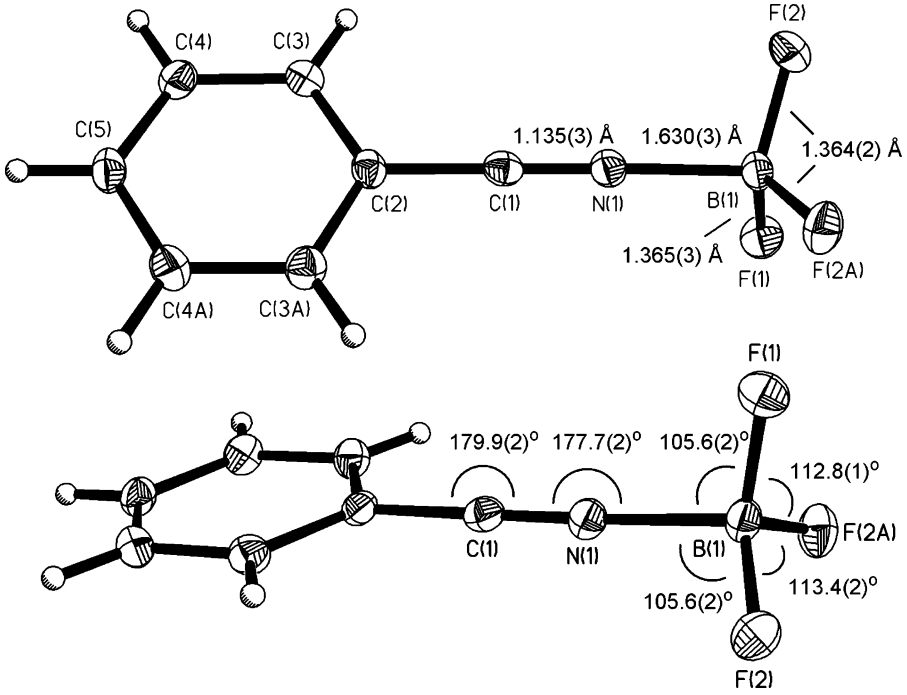

Figure 2. Thermal ellipsoid representations (50% probability boundaries) of the X-ray crystal structure of $C_6H_5CN-BF_3$, with significant interatomic distances (top) and angles (bottom) noted. Atom pairs F(2)−F(2A), C(3)−C(3A), and C(4)−C(4A) are related by a crystallographic mirror plane.

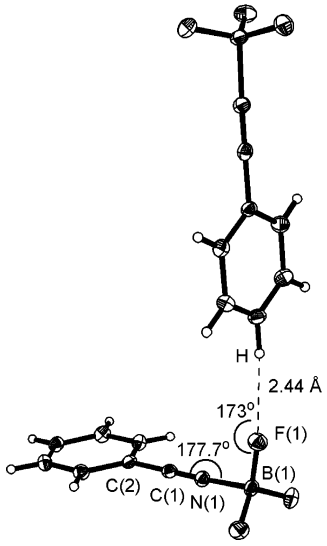

Figure 3. Intermolecular interaction of neighboring $C_6H_5CN-BF_3$ complexes in the solid state.

common. One particularly relevant example is observed in the BF_3 adduct of a cyanide ligand in a transition metal complex, $[HRu(DPPE)_2CN-BF_3]\cdot CH_2Cl_2$.[30] In this complex, the BF_3 unit participates in a slightly shorter intermolecular B−F···H interaction (2.38 Å) with a nearby phenyl ring, resulting in bending of the C≡N−B unit to 172.5°.

Frequencies. The identification and assignment of vibrational bands for matrix-isolated $C_6H_5CN-BF_3$ and $(CH_3)_3CCN-BF_3$ was facilitated greatly by our previous work on CH_3CN-BF_3 in solid argon.[11] In general, all bands assigned to the 1:1 complexes were initially identified because they were observed only when both BF_3 and nitrile were present, grew slightly upon annealing, and were observed at frequencies very near those of the corresponding modes of CH_3CN-BF_3. Mode assignments were ultimately based on $^{10}B-^{11}B$ isotope shifts and consistent sets of relative intensities across all experimental conditions studied. Frequencies for the experimentally observed bands for both $C_6H_5CN-BF_3$ and $(CH_3)_3CCN-BF_3$ are listed in Tables 3 and 4 (below), respectively, together with those calculated from the gas-phase complexes.

In $C_6H_5CN-BF_3$ experiments, bands requiring both BF_3 and C_6H_5CN were observed at 2320, 1253, 1295, 848, 602, and 590 cm^{-1}. All of these features grew slightly upon annealing to 25 K. An additional band was also observed at 874 cm^{-1}, but only when matrices were deposited above 12 K, or after those deposited at lower temperatures were annealed. Representative spectra showing the regions of these absorption features are displayed Figure 4, and peaks definitively assigned to the 1:1, $C_6H_5CN-BF_3$ complex are noted with asterisks and are included in Table 4. The pair at 1253 and 1290 cm^{-1} were immediately recognized as a $^{10}B-^{11}B$ isotopic pair due to the characteristic intensity ratio, and a splitting (47 cm^{-1}) that compared favorably with the computed isotope shift (48 cm^{-1}, below), as well as those measured for gas-phase BF_3 (51 cm^{-1})[19] and matrix-isolated CH_3CN-BF_3 (45 cm^{-1}).[11] Thus, the peaks at 1253 and 1290 cm^{-1} were assigned to the BF asymmetric stretching modes (ν^a_{BF}) of $C_6H_5CN-^{11}BF_3$ and $C_6H_5CN-^{10}BF_3$, respectively. The peaks at 590 and 602 cm^{-1} also exhibited an intensity ratio characteristic of a $^{11}B-^{10}B$ isotopic pair and a splitting (12 cm^{-1}) consistent with that of the BF symmetric bend or "umbrella" mode (δ^a_{BF}) as predicted by computations (13 cm^{-1}, below) and in previous measurements of this band for CH_3CN-BF_3 (16 cm^{-1}).[11] Given this, and consistent intensities relative

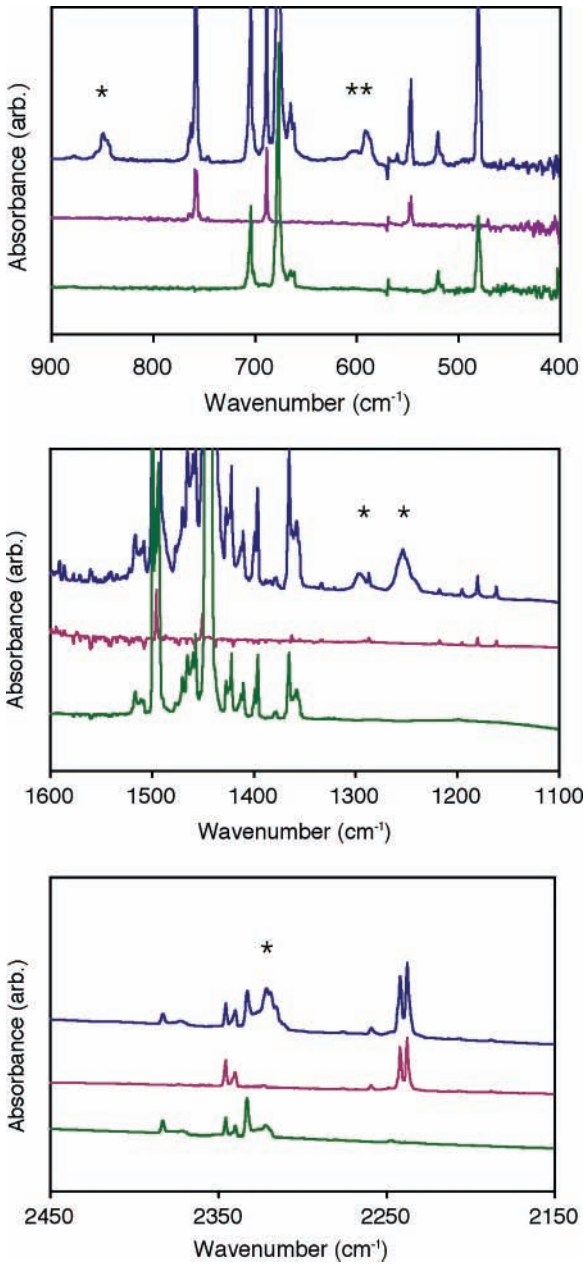

Figure 4. IR spectra showing the absorption bands of $C_6H_5CN-BF_3$ in solid argon at 10 K. Bottom traces: BF_3 in argon, 1:400. Middle traces: C_6H_5CN in solid argon, approximately 1:400. Spectrum was obtained by mixing C_6H_5CN vapor into a stream of pure argon immediately prior to deposition. Top traces: BF_3 and C_6H_5CN in argon, approximately 1:1:400, obtained by mixing C_6H_5CN vapor into a stream of BF_3 and argon. Peaks assigned to $C_6H_5CN-BF_3$ are marked with asterisks.

to the asymmetric stretching bands, the peaks at 590 and 602 cm^{-1} were assigned to the umbrella modes of the ^{11}B and ^{10}B isotopomers of $C_6H_5CN-BF_3$, respectively. The peak at 2320 cm^{-1} occurs about 80 cm^{-1} higher in frequency than the CN stretching bands observed for C_5H_5CN, which compares favorably with blue-shifts observed for various other CH_3CN complexes.[10] No $^{11}B-^{10}B$ isotope shift is predicted for the CN stretching band of $C_6H_5CN-BF_3$ (below), and none was observed previously for CH_3CN-BF_3. The 2320 cm^{-1} band did exhibit reasonably consistent intensities relative to those assigned above, despite being partially obscured by background CO_2 in many experiments. Thus, we ultimately assigned the peak at 2320 to the CN stretching band (ν_{CN}) of the complex. The band

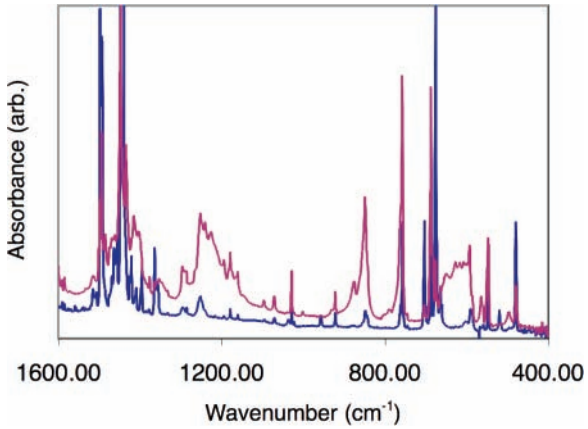

Figure 5. IR spectrum of a 1:1:400 sample of BF_3 and C_6H_5CN in argon at 10 K before (bottom) and after (top) annealing to 35 K for 30 min.

at 848 cm^{-1} lies in the region of the BF_3 symmetric stretch, which is forbidden in free BF_3[31] but can become rather strong when the BF_3 moiety is distorted to a pyramidal geometry.[14] This band also has consistent intensities relative to those of the other bands discussed, and a very small $^{10}B-^{11}B$ isotope shift is predicted (below), so the band at 848 cm^{-1} was assigned to the B−F symmetric stretch of $C_6H_5CN-BF_3$.

A group of broad features appeared near those discussed above when matrices were annealed to fairly high temperatures, about 35 K, and as such, these are presumably due to larger aggregates of C_6H_5CN and BF_3 (i.e., either $(C_6H_5CN-BF_3)_n$ or $(C_6H_5CN)_m(BF_3)_n$). This claim is supported by the fact that these features appear in the regions between the bands assigned to the 1:1 complexes and those observed for the bulk solids in "matrix-free" experiments (below). Furthermore, they are shifted relative to those assigned to the 1:1 complex in a manner that is consistent with species having B−N dative bonds compressed relative to isolated $C_6H_5CN-BF_3$,[13] which would be expected on the basis of the medium-induced structural changes noted above. A spectrum displaying these broad absorption features is shown in Figure 5, and it should be noted that no clearly resolved peaks could be distinguished within these regions, nor could any peaks that could be associated with specific clusters. Peak maxima did occur on the broad feature near the asymmetric stretch at 1288, 1240, and 1226 cm^{-1} near the umbrella band at 649, 628, 607, and 600 cm^{-1}, and another band also grows in just to the blue of the CN stretch at 2330 cm^{-1}. The band at 874 cm^{-1}, initially observed when matrices were deposited above 12 K, also grew very rapidly upon annealing to 35 K, and thus is likely due to larger aggregates as well.

The rationale by which the IR bands were assigned to $(CH_3)_3CCN-BF_3$ in argon matrix experiments was essentially identical to that for $C_6H_5CN-BF_3$. Bands requiring both BF_3 and $(CH_3)_3CCN$ were observed at 2323, 1247, 1290, 840, 617, and 603 cm^{-1}. Secondary peaks were observed for nearly all of these bands, presumably due to distinct trapping sites in the matrix. The spectral regions in which these bands occur are displayed in Figure 6, and bands definitively assigned to the 1:1 complex are marked with asterisks. Frequencies, including both peak maxima observed for bands that were split, are listed in Table 4. The pair at 1290 and 1247 cm^{-1} was assigned to the asymmetric stretching bands of the ^{10}B and ^{11}B isotopomers, respectively, on the basis of the observed splitting (43 cm^{-1}). It is worth noting that a relatively strong band of $(CH_3)_3CCN$ almost completely obscures the ^{11}B component, and this prevented any reliable measurement of the peak area. The bands

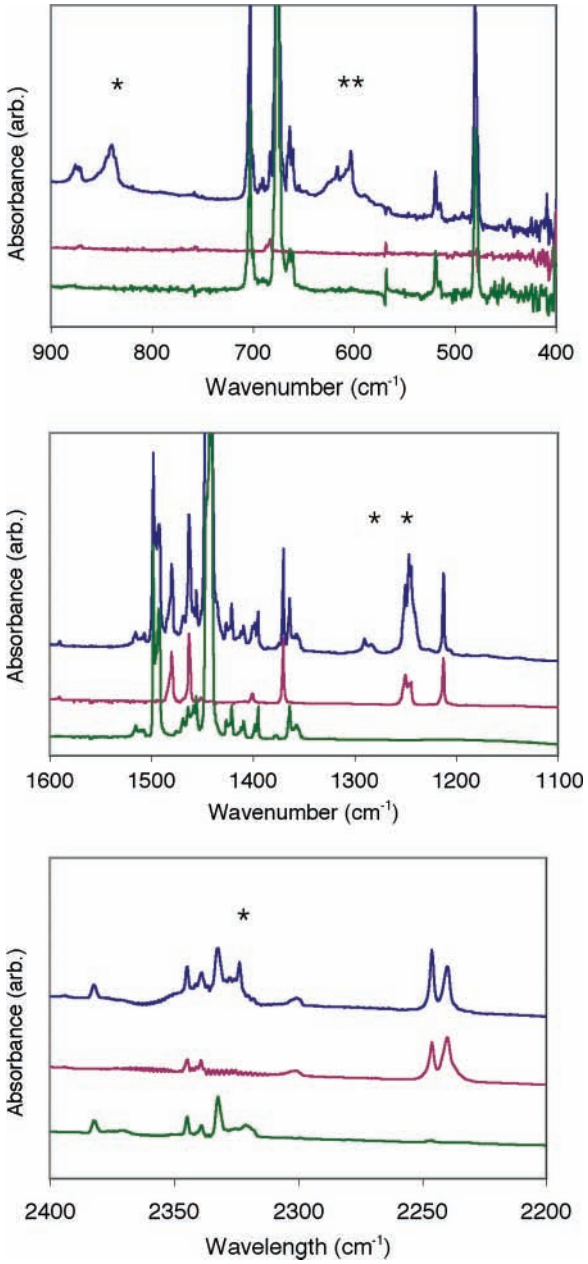

Figure 6. Representative IR spectra showing the absorption bands of $(CH_3)_3CCN-BF_3$ in solid argon at 13 K. Bottom trace: BF_3 in argon, 1:400. Middle trace: $(CH_3)_3CCN$ in solid argon, 1:400. Top trace: BF_3 and C_6H_5CN in argon, approximately 1:1:800. Peaks assigned to $C_6H_5CN-BF_3$ are marked with asterisks.

at 617 and 603 cm^{-1} were assigned to the umbrella modes of the ^{10}B and ^{11}B isotopomers, respectively, on the basis of the isotope splitting (14 cm^{-1}) and relative intensities. The band at 2323 cm^{-1} was assigned to the CN stretch on the basis of relative intensities and the characteristic blue shift relative to the CN stretching band of $(CH_3)_3CCN$. An additional band was also measured at 875 cm^{-1}, but it was only observed upon annealing, or in warmer depositions (above 12 K), much like the band observed near this frequency in the benzonitrile/BF_3 experiments.

There are significant differences between the matrix frequencies and those observed in the spectra of matrix-free, bulk solid samples. IR spectra of the bulk solids resulting from codeposition of C_6H_5CN or $(CH_3)_3CCN$ with BF_3 are displayed in Figures 7 and 8, and observed frequencies of the major bands are listed Tables 3 and 4, respectively. In general, the spectra

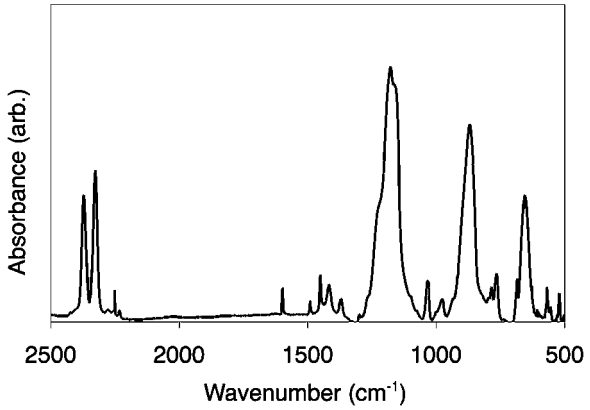

Figure 7. IR spectrum of a bulk solid sample of BF_3 and C_6H_5CN codeposited at 100 K.

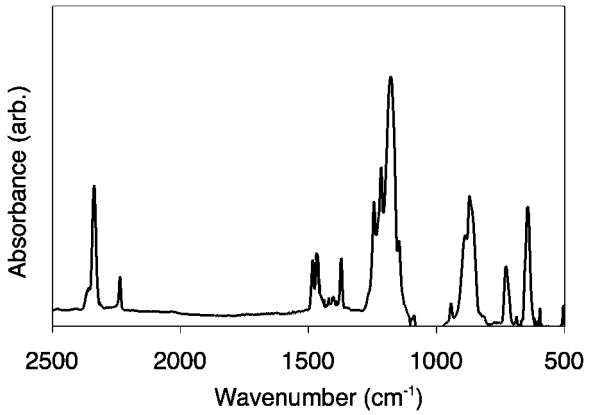

Figure 8. IR spectrum of a bulk solid sample of BF_3 and $(CH_3)_3CCN$ codeposited at 100 K.

very closely resemble the solid-state IR spectrum of CH_3CN-BF_3,[12] which is dominated by three strong bands near 1200, 880, and 650 cm^{-1} that correspond to the BF_3 asymmetric stretch, the BF_3 symmetric stretch, and the BF_3 umbrella mode, respectively. The CN stretch is also reasonably strong in those spectra,[12] and it is observed at 2376 cm^{-1}, but all other bands of CH_3CN-BF_3 (s) are quite weak in comparison to these. Given the similarities between the spectra shown in Figures 7 and 8 and the CH_3CN-BF_3 data, not only in terms of frequencies but also relative band intensities, it is presumed that the dominant bands can be assigned by comparison to CH_3CN-BF_3 and that peak frequencies correspond to those of the ^{11}B isotopomer, which comprises 81% of the sample. In the solid-state $C_6H_5CN-BF_3$ spectrum, the BF asymmetric stretch is observed at 1177 cm^{-1}, the BF symmetric stretch at 868 cm^{-1}, and the umbrella mode at 654 cm^{-1}. These differ from the corresponding band in the matrix by −76, +20, and +64 cm^{-1}, respectively. The CN stretch is observed as a doublet, just to the blue of the matrix frequencies, at 2328 and 2374 cm^{-1}. The underlying reasons for the doubling were not pursued, but we note that the 2328 peak is essentially coincident with the matrix band, while the latter is shifted about 50 cm^{-1} to the blue. All of these shifts, with the possible exception of the one CN stretching doublet, are consistent with the idea that the matrix-isolated complex has a weaker intramolecular bond with a longer B−N distance than its crystalline counterpart.[13]

In the solid-state $(CH_3)_3CCN-BF_3$ spectrum, the BF_3 asymmetric stretch is observed at 1172 cm^{-1}, the BF_3 symmetric stretch at 865 cm^{-1}, the umbrella mode at 654 cm^{-1}, and the CN stretch is observed at 2340 cm^{-1}. These differ from the corresponding bands in the matrix by −75, +25, +34, and +17 cm^{-1}, respectively. The solid-state frequencies, as well as the relative band intensities are quite similar to those observed for $C_6H_5CN-BF_3$ (s) and CH_3CN-BF_3 (s), and this suggests that the solid-state structure of $(CH_3)_3CCN-BF_3$ is also similar to that of those species. This is significant in this case, because no X-ray structure for $(CH_3)_3CCN-BF_3$ could be obtained. Again, the shifts observed relative to the matrix data are consistent with the idea that the matrix-isolated complex is more weakly bonded and has a longer B−N distance than its solid-state counterpart.

Computed (B3LYP/aug-cc-pV(T|D)Z) frequencies of the experimentally observed bands are included in Tables 3 and 4, while the complete lists, including intensities, symmetry labels, and approximate mode descriptions are included as Supporting Information (Tables S2 and S3). A somewhat unusual scaling procedure for these frequencies, used previously for CH_3CN-BF_3,[13] was adopted in order to facilitate agreement between experiment and theory for CH_3CN and BF_3. That is, all frequencies above 2000 cm^{-1} are scaled by a factor of 0.96, but all others are left unscaled. Thus, the CN stretch is the only mode of interest affected by this procedure. In general, the calculated frequencies differ only slightly from the measured matrix bands, by less than 20 cm^{-1} in almost every instance. However, the differences are systematic, in that gas-to-matrix shifts are consistent with the idea that the matrix does offer stabilization for the complexes and, in turn, causes a slight

TABLE 3: Observed and Calculated[a] Vibrational Frequencies of $C_6H_5CN-BF_3$

			frequency (cm^{-1})	
mode	description	phase	$C_6H_5CN-{}^{11}BF_3$	$C_6H_5CN-{}^{10}BF_3$
$\delta_{BF}{}^{A}$	B−F symmetric deformation or "umbrella" mode	gas (B3LYP)	585	598
		Ar matrix	590	602
		solid	654	
$\nu_{BF}{}^{S}$	BF_3 symmetric stretch	gas (B3LYP)	843	848
		Ar matrix	848	848
		solid	868	
$\nu_{BF}{}^{A}$	BF_3 asymmetric stretch[b]	gas (B3LYP)	1266	1314
		Ar matrix	1253	1295
		solid	1177	
ν_{CN}	C−N stretch	gas (B3LYP)	2300	2300
		Ar matrix	2320	2320
		solid	2328/2374	

[a] Frequencies were calculated using the B3LYP/aug-cc-pVT|D)Z method, and frequencies above 2000 cm^{-1} were scaled by a factor of 0.96. See text for discussion. [b] This mode is not formally degenerate in the complex, as it is in free BF_3, because of lower symmetry, but the calculated splitting is only 0.1 cm^{-1}.

TABLE 4: Observed and Calculated[a] Vibrational Frequencies of $(CH_3)_3CCN-BF_3$

			frequency (cm^{-1})	
mode	description	phase	$(CH_3)_3CCN-{}^{11}BF_3$	$(CH_3)_3CCN-{}^{10}BF_3$
$\delta_{BF}{}^{A}$	B−F symmetric deformation or "umbrella" mode	gas (B3LYP)	585	601
		Ar matrix	603/607	617/621
		solid	637	
$\nu_{BF}{}^{S}$	BF_3 symmetric stretch	gas (B3LYP)	834	840
		Ar matrix	840	840
		solid	865	
$\nu_{BF}{}^{A}$	BF_3 asymmetric stretch	gas (B3LYP)	1258	1304
		Ar matrix	1247	1290
		solid	1172	
ν_{CN}	C−N stretch	gas (B3LYP)	2313	2313
		Ar matrix	2323/2327	2323
		solid	2340	

[a] Frequencies were calculated using the B3LYP/aug-cc-pV(T|D)Z method, and frequencies above 2000 cm^{-1} were scaled by a factor of 0.96. See text for discussion.

contraction of the B−N bonds. Given that these observed shifts are only slightly larger than the differences usually observed between matrix and gas-phase frequencies, typically 10 cm^{-1},[32] this cannot be considered definitive evidence for a matrix effect on the structure of these complexes. In any event, the data are consistent with some slight matrix-induced structural changes, though certainly much less extreme than those depicted by the analogous data for CH_3CN-BF_3.[11,13]

In comparing frequencies for $C_6H_5CN-BF_3$, $(CH_3)_3CCN-BF_3$ and CH_3CN-BF_3 within a given medium, it is clear that variations in the degree to which these species are affected by various condensed-phase environments stem mainly from differences in structural properties of the gas-phase species. Indeed, matrix frequencies for the BF_3-localized modes among all three complexes are quite consistent, suggesting that the structures of the complexes are similar in solid argon, at least in regard to the effects on the BF_3 moiety. For example, the BF_3 asymmetric stretching frequencies for the ^{11}B isotopomers of $C_6H_5CN-BF_3$, $(CH_3)_3CCN-BF_3$, and CH_3CN-BF_3 in solid argon are 1253, 1247, and 1249 cm^{-1}, and those of the umbrella modes are 590, 603, and 601 cm^{-1}, respectively. The frequencies of the solid-state complexes are nearly as consistent, and furthermore, all of the known crystal structures of $RCN-BF_3$-type complexes[7,9] have nearly identical structures about the nitrile and BF_3 subunits (aside from the slight bend in $C_6H_5CN-BF_3$ (s)). Very slight gas-phase structure differences were noted above, and indeed, the calculated frequencies of $C_6H_5CN-BF_3$ and $(CH_3)_3CCN-BF_3$ do reflect shifts that parallel these subtle differences, as expected on the basis of how calculated CH_3CN-BF_3 frequencies shift with B−N distance.[13] For CH_3CN-BF_3, there are two minimum-energy structures at the B3LYP/aug-cc-pVQZ level of theory, with B−N distances of 1.919 and 2.319 Å, the latter being lower in energy by only 0.11 kcal/mol. For the shorter structure, the frequencies of the BF_3 asymmetric stretching and BF_3 umbrella bands are 1306 and 564 cm^{-1}, respectively (for the ^{11}B isotopomer). These are significantly different from the analogous frequencies of $C_6H_5CN-BF_3$ and $(CH_3)_3CCN-BF_3$ listed in Tables 3 and 4, and the shifts parallel the differences in predicted structure between CH_3CN-BF_3 and the two complexes with larger organic substituents. However, intermolecular interactions exert a stabilizing effect that apparently nullifies the gas-phase structural differences, and in turn, frequencies measured in the matrix and crystalline environments reflect structures that are quite similar.

B−N Potential Energy Curves. The differences in the extent to which condensed-phase environments affect the structure and bonding of CH_3CN-BF_3, $C_6H_5CN-BF_3$, and $(CH_3)_3CCN-BF_3$ are further illustrated by a comparison of B−N distance potential curves. Curves obtained using the B3LYP method with a variety of basis sets are shown in Figures 9 and 10 for $C_6H_5CN-BF_3$ and $(CH_3)_3CCN-BF_3$, respectively. The zero of energy for these plots were chosen to be the lowest point on the curve, as the overall shape relative to the minimum is the main concern. In general, they are all fairly flat, especially the $C_6H_5CN-BF_3$ curves, and both exhibit the key features observed previously for CH_3CN-BF_3, including signs of two distinct minima near 1.8 and 2.3 Å, and a peculiar sensitivity to diffuse functions in

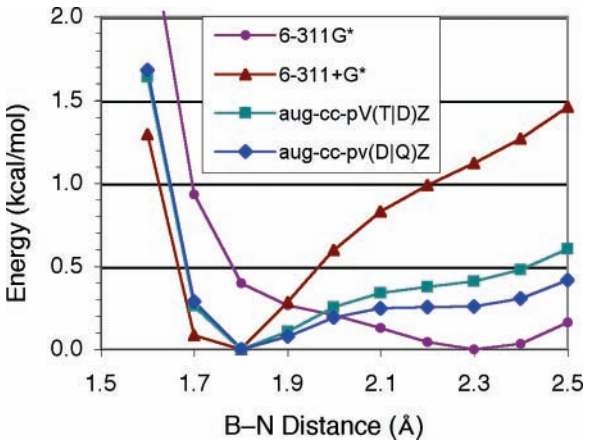

Figure 9. Electronic energy of $C_6H_5CN-BF_3$ versus B−N distance using the B3LYP method and various basis sets.

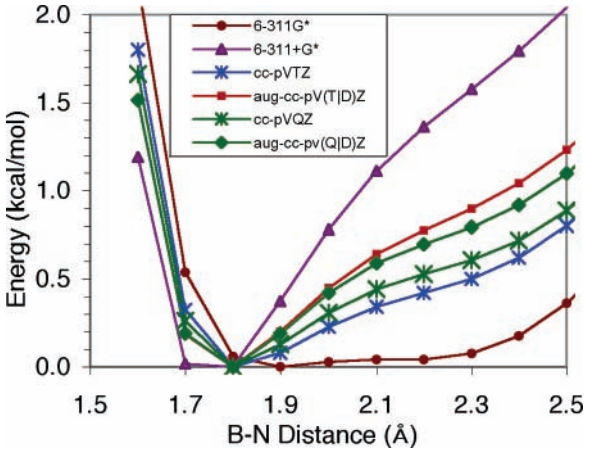

Figure 10. Electronic energy of $(CH_3)_3CCN-BF_3$ versus B−N distance using the B3LYP method and various basis sets.

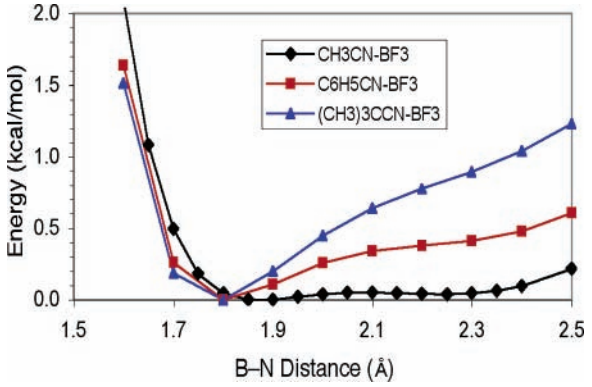

Figure 11. The B−N distance potentials of CH_3CN-BF_3, $C_6H_5CN-BF_3$, and $(CH_3)_3CCN-BF_3$, calculated at the B3LYP/aug-cc-pVTZ (CH_3CN-BF_3) or B3LYP/aug-cc-pV(T|D)Z (others) level of theory.

the basis set. For CH_3CN-BF_3, the minima occur near 1.8 Å, and there is a shelflike region near 2.3 Å when diffuse functions are included in the basis set. In the absence of diffuse functions, as well as with the largest basis set used (aug-cc-pVQZ), the global minimum resides in the 2.3 Å region, and a shelflike feature occurs near 1.8 Å.[13] The $C_6H_5CN-BF_3$ curves follow the same general trend, but the basis set effect is not as distinct for $(CH_3)_3CCN-BF_3$. It is perhaps most apparent upon comparison of the 6-311G* and 6-311+G* data. For the former, the potentials are quite flat, and for $C_6H_5CN-BF_3$, the global minimum occurs in the outer region near 2.3 Å. For $(CH_3)_3CCN-BF_3$, the 6-311G* curve is still quite flat, but the global minimum is still near 1.8 Å, like all others. In contrast, the 6-311+G* curves are steeper and depict a structure that would be more localized in the 1.8 Å region for both complexes. For the larger basis sets, the curves lie between the 6-311G* and 6-311+G* data, but those that lack diffuse functions (Figure 10 only) are indeed flatter and systematically lower in energy in the 2.3 Å region.

The curves are not as flat as those obtained previously for CH_3CN-BF_3,[13] however. For $C_6H_5CN-BF_3$ at the B3LYP/aug-cc-pV(Q|D)Z level, the potential is at or below 0.3 kcal/mol for 0.7A, from just beyond 1.7 Å to 2.4 Å. For $(CH_3)_3CCN-BF_3$ the curves are much steeper. At the B3LYP/aug-cc-pV(Q|D)Z level, the curve remains under 0.3 kcal/mol for only about 0.3 Å. A comparison of the B3LYP/aug-cc-pVQZ and B3LYP/aug-cc-pV(Q|D)Z curves for CH_3CN-BF_3, $C_6H_5CN-BF_3$, and $(CH_3)_3CCN-BF_3$ is shown in Figure 11, and it illustrates the very subtle effects that the larger organic substituents exert on the structures of these systems. Clearly, the $(CH_3)_3CCN-BF_3$ curve is steepest and depicts a structure that is very much localized in the 1.8 Å region. The CH_3CN-BF_3 curve is quite flat, and in fact, the experimental, vibrationally averaged gas-phase B−N distance lies near the middle of the flat region at 2.01 Å.[3] The $C_6H_5CN-BF_3$ curve lies between the other two but is also quite flat in the 2.1−2.3 Å region. Thus, with larger organic substituents, the inner region of the potential is stabilized relative to the 2.3 Å region, and in turn, the structures are more localized near 1.8 Å. Ultimately, the medium effects on the structure of the two larger complexes are more muted because the inner region is more stable even in the absence of any interactions with some condensed-phase environment. By contrast, condensed-phase interactions must stabilize the inner region of the very flat CH_3CN-BF_3 potential relative to the outer 2.3 Å region because the complex is more polar at shorter B−N distances,[13] which would drive the medium-induced structural changes.

V. Summary and Conclusions

Condensed-phase effects on the structure and bonding of $C_6H_5CN-BF_3$ and $(CH_3)_3CCN-BF_3$ have been illustrated by a myriad of data, and these have been compared and contrasted to analogous results for the closely related complex CH_3CN-BF_3. For the most part, the structural properties of $C_6H_5CN-BF_3$ and $(CH_3)_3CCN-BF_3$ are similar, not only in the gas phase but also in the solid state and in argon matrices. There is clear evidence, however, that these structures do change significantly from medium to medium. The measured crystallographic structure of $C_6H_5CN-BF_3$ (s) differs markedly from the equilibrium gas-phase structure obtained via B3LYP calculations, though these differences are somewhat less extreme than those observed for $HCN-BF_3$[9] and CH_3CN-BF_3.[7] Furthermore, the IR spectrum of $(CH_3)_3CCN-BF_3$ (s) suggests that its solid-state structure resembles those of CH_3CN-BF_3 and $C_6H_5CN-BF_3$, and in turn, that there is a significant gas−solid structure difference for this complex as well. Notable differences between calculated gas-phase frequencies and measured solid-state frequencies for both $C_6H_5CN-BF_3$ and $(CH_3)_3CCN-BF_3$ have been also observed, and the shifts are consistent with those expected on the basis of the structural changes.[13] Frequencies measured in argon matrices were found to be quite similar for both complexes and also very near those measured previously for CH_3CN-BF_3, suggesting that all three complexes adopt similar structures, at least about the BF_3 moiety, in the inert matrix environment. This is although there are significant differences between the calculated gas-phase structures of CH_3CN-BF_3 and the two complexes with larger organic substituents. For $C_6H_5CN-BF_3$ and $(CH_3)_3CCN-BF_3$, matrix IR frequencies differ only slightly from the computed gas-phase values, but they are shifted systematically in a manner that suggests a slight compression of the B−N bond relative to the gas phase. By contrast, there are large differences between matrix and calculated gas-phase frequencies for CH_3CN-BF_3.[11,13] Since both IR spectra and available crystallographic data indicate that the structures of CH_3CN-BF_3, $C_6H_5CN-BF_3$, and $(CH_3)_3CCN-BF_3$ are similar in the solid-state and matrix environments, it appears that the varying degree to which these systems are affected by condensed phases stems ultimately from subtle differences in gas-phase structural properties. These differences were highlighted through an examination of B−N distance potentials obtained from B3LYP calculations using a variety of basis sets. In general, curves for all three species are somewhat flat, and indeed, those for both $C_6H_5CN-BF_3$ and $(CH_3)_3CCN-BF_3$ show signs of the two distinct minima exhibited in the B−N potential of CH_3CN-BF_3. However, the larger organic substituents seem to cause a greater stabilization of the inner region of the potential, such that the structures are more localized in the 1.8 Å region, even in the absence of interactions with a bulk, condensed-phase medium. Thus, while $C_6H_5CN-BF_3$ and $(CH_3)_3CCN-BF_3$ do share some of the peculiarities exhibited by CH_3CN-BF_3, the structural changes induced by condensed-phase environments are less extreme.

Acknowledgment. J.A.P. Gratefully acknowledges the National Science Foundation (CHE-0216058 and CHE-0407824) for financial support of this work, as well as the donors of the ACS Petroleum Research Fund (37834-B6), and Research Corporation (CC5622). Additional support was provided by Office of Research and Sponsored Programs at the University of Wisconsin−Eau Claire.

Supporting Information Available: Crystallographic information file (Table S1), a stereoscopic projection of the

$C_6H_5CN-BF_3$ unit cell (Figure S1), and computed frequencies of $C_6H_5CN-BF_3$ (Table S2) and $(CH_3)_3CCN-BF_3$ (Table S3). This material is available free of charge via the Internet at http://pubs.acs.org.

References and Notes

(1) Leopold, K. R.; Canagaratna, M.; Phillips, J. A. *Acc. Chem. Res.* **1997**, *30*, 57.

(2) Leopold, K. R. In *Advances in Molecular Structure Research*; Hargittai, M., Hargittai, I., Eds.; JAI Press: Greenwich, CT 1996; Vol. 2.

(3) Dvorak, M. A.; Ford, R. S.; Suenram, R. D.; Lovas, F. J.; Leopold, K. R. *J. Am. Chem. Soc.* **1992**, *114*, 108.

(4) Fujiang, D.; Fowler, P. W.; Legon, A. C. *J. Chem. Soc., Chem. Commun.* **1995**, 113.

(5) Janda, K. C.; Bernstien, L. S.; Steed, J. M.; Novick, S. E.; Klemperer, W. *J. Am. Chem. Soc.* **1978**, *100*, 8074.

(6) Leopold, K. R.; Fraser, G. T.; Klemperer, W. *J. Am. Chem. Soc.* **1978**, *100*, 8074.

(7) Swanson, B.; Shiver, D. F.; Ibers, J. A. *Inorg. Chem.* **1969**, *8*, 2183.

(8) Reeve, S. W.; Burns, W. A.; Lovas, F. J.; Suenram, R. D.; Leopold, K. R. *J. Phys. Chem.* **1993**, *97*, 10630.

(9) Burns. W. A.; Leopold, K. R. *J. Am. Chem. Soc.* **1993**, *115*, 11622.

(10) (a) Purcell, K. F.; Drago, R. S. *J. Am. Chem. Soc.* **1966**, *88*, 919. (b) Coerver, H. J.; Curran, C. *J. Am. Chem. Soc.* **1958**, *80*, 3522.

(11) Wells, N. P.; Phillips, J. A. *J. Phys. Chem. A* **2002**, *106*, 1518.

(12) Swanson, B.; Shriver, D. F. *Inorg. Chem.* **1970**, *9*, 1406.

(13) Giesen, D. J.; Phillips, J. A. *J. Phys Chem. A* **2003**, *107*, 4009.

(14) Cho, H-.G.; Cheong, B.-S. *THEOCHEM* **2000**, *496*, 185.

(15) Jurgens, R.; Almlöf, J. *Chem. Phys. Lett.* **1991**, *176*, 263.

(16) Jiao, H. J.; Schleyer, P. v. R. *J. Am. Chem. Soc.* **1994**, *116*, 7429.

(17) Jonas, V.; Frenking, G.; Reetz, M. T. *J. Am. Chem. Soc.* **1994**, *116*, 8741.

(18) *The NIST Chemistry Webbook*; http://webbook.nist.gov/chemistry (accessed December 2004).

(19) Harms, K. *XCAD4: Program for the Lp-correction of CAD4/Mach3 Diffractometer Data*; University of Marburg: Marburg, Germany, 1996.

(20) *SHELXTL NT* v. 6.12; Bruker AXS: Madison WI 2001.

(21) Frisch, M. J.; Trucks, G. W.; Schlegel, H. B.; Scuseria, G. E.; Robb, M. A.; Cheeseman, J. R.; Zakrzewski, V. G.; Montgomery, J. A., Jr.; Stratmann, R. E.; Burant, J. C.; Dapprich, S.; Millam, J. M.; Daniels, A. D.; Kudin, K. N.; Strain, M. C.; Farkas, O.; Tomasi, J.; Barone, V.; Cossi, M.; Cammi, R.; Mennucci, B.; Pomelli, C.; Adamo, C.; Clifford, S.; Ochterski, J.; Petersson, G. A.; Ayala, P. Y.; Cui, Q.; Morokuma, K.; Malick, D. K.; Rabuck, A. D.; Raghavachari, K.; Foresman, J. B.; Cioslowski, J.; Ortiz, J. V.; Stefanov, B. B.; Liu, G.; Liashenko, A.; Piskorz, P.; Komaromi, I.; Gomperts, R.; Martin, R. L.; Fox, D. J.; Keith, T.; Al-Laham, M. A.; Peng, C. Y.; Nanayakkara, A.; Gonzalez, C.; Challacombe, M.; Gill, P. M. W.; Johnson, B. G.; Chen, W.; Wong, M. W.; Andres, J. L.; Head-Gordon, M.; Replogle, E. S.; Pople, J. A. *Gaussian 98*, revision A9; Gaussian, Inc.: Pittsburgh, PA, 1998.

(22) Frisch, M. J.; Trucks, G. W.; Schlegel, H. B.; Scuseria, G. E.; Robb, M. A.; Cheeseman, J. R.; Montgomery, Jr., J. A.; Vreven, T.; Kudin, K. N.; Burant, J. C.; Millam, J. M.; Iyengar, S. S.; Tomasi, J.; Barone, V.; Mennucci, B.; Cossi, M.; Scalmani, G.; Rega, N.; Petersson, G. A.; Nakatsuji, H.; Hada, M.; Ehara, M.; Toyota, K.; Fukuda, R.; Hasegawa, J.; Ishida, M.; Nakajima, T.; Honda, Y.; Kitao, O.; Nakai, H.; Klene, M.; Li, X.; Knox, J. E.; Hratchian, H. P.; Cross, J. B.; Bakken, V.; Adamo, C.; Jaramillo, J.; Gomperts, R.; Stratmann, R. E.; Yazyev, O.; Austin, A. J.; Cammi, R.; Pomelli, C.; Ochterski, J. W.; Ayala, P. Y.; Morokuma, K.; Voth, G. A.; Salvador, P.; Dannenberg, J. J.; Zakrzewski, V. G.; Dapprich, S.; Daniels, A. D.; Strain, M. C.; Farkas, O.; Malick, D. K.; Rabuck, A. D.; Raghavachari, K.; Foresman, J. B.; Ortiz, J. V.; Cui, Q.; Baboul, A. G.; Clifford, S.; Cioslowski, J.; Stefanov, B. B.; Liu, G.; Liashenko, A.; Piskorz, P.; Komaromi, I.; Martin, R. L.; Fox, D. J.; Keith, T.; Al-Laham, M. A.; Peng, C. Y.; Nanayakkara, A.; Challacombe, M.; Gill, P. M. W.; Johnson, B.; Chen, W.; Wong, M. W.; Gonzalez, C.; Pople, J. A. *Gaussian 03*, Revision B.05; Gaussian, Inc., Wallingford CT, 2004.

(23) Binkley, J. S.; Pople, J. A.; Hehre, W. J. *J. Am. Chem. Soc.* **1980**, *102*, 939.

(24) Easton, R. E.; Giesen, D. J.; Welch, A.; Cramer, C. J.; Truhlar, D. G. *Theor. Chim. Acta* **1996**, *93*, 281.

(25) Hehre, W. J.; Ditchfield, R.; Pople, J. A. *J. Chem. Phys.* **1972**, *56*, 2257.

(26) Krishnan, R.; Binkley, J. S.; Seeger, R.; Pople, J. A. *J. Chem. Phys.* **1980**, *72*, 650.

(27) McLean, A. D.; Chandler, G. S. *J. Chem. Phys.* **1980**, *72*, 5639.

(28) Woon, D. E.; Dunning, T. H., Jr. *J. Chem. Phys.* **1993**, *98*, 1358.

(29) Allen, F. H. *Acta Crystallogr.* **2002**, *B58*, 380−388.

(30) Rocchini, E.; Rigo, P.; Mezzetti, A.; Stephan, T.; Morris, R. H.; Lough, A. J.; Forde, C. E.; Fong, T. P.; Drouin, S. D. *J. Chem. Soc., Dalton Trans.* **2000**, 3591−3602.

(31) Herzberg, G. *Molecular Spectra and Molecular Structure, Volume II, Infrared and Raman Spectra of Polyatomic Molecules;* Krieger Publishing Co.: Malabar, FL, 1991.

(32) See for example: Dunkin, I. R. *Matrix Isolation Techniques: A Practical Approach*; Oxford University Press: Oxford, 1998.